Electronic Supplementary Information

$Na_{1.5}Rb_{0.5}PO_3F \cdot H_2O$: synthesis, properties, and stepwise reconstruction of the hydrogen bond network

Xin-Rui Yang,[a] Xin Liu,[a] Zujian Wang,[b] Xue-Bin Deng,[a] He-Jie Lu,[a] Yu-Jia Li,[a] Xifa Long,[b] Ling Chen*[a] and Li-Ming Wu*[a]

[a]*Beijing Key Laboratory of Energy Conversion and Storage Materials, College of Chemistry, Beijing Normal University, Beijing 100875, People's Republic of China*

[b]*Key Laboratory of Optoelectronic Materials Chemistry and Physics, State Key Laboratory of Structure Chemistry, Fujian Institute of Research on the Structure of Matter, Chinese Academy of Sciences, Fuzhou, Fujian 350002, People's Republic of China*

Contents

I. Experimental Section

Powder X-ray Diffraction (PXRD). The data was collected at room temperature on a Bruker Model D8 Advance powder X-ray diffractometer equipped, using Cu Kα radiation source (λ = 1.5418 Å) with a scan step width of 0.02°. The 2θ spans over 5–80° with a step of 0.1 s. The sample was tested on a quartz sample holder, whereas the residual after the thermal analysis was tested on a zero background sample holder. An X-ray orientator (Dandong Co., model: YX-2) and the corresponding XRD patterns were used to examine the major facets of the $NRPF{\cdot}H_2O$ single crystal after simple hand-polishing on a zero background sample holder.

Single-Crystal Structure Determination. The single-crystal X-ray diffraction data was collected on a Bruker PHOTON II CPAD detector with a mirror-monochromatic INCOATEC IμS microfocus radiation source (50 kV per 1.4 mA).

Thermal Stability. Thermogravimetric and differential scanning calorimetry (TG and DSC) curves were carried out on a NETZSCH STA449 F5 analyzer at a rate of 20 K/min from 30 to 450 °C under the nitrogen atmosphere with an Al_2O_3 crucible containing the powder sample about 4–8 mg.

Ultraviolet–Visible–Near Infrared (UV–vis–NIR) Diffuse Reflectance and Infrared (IR) Spectra. The diffuse spectra was measured from 200 to 1400 nm on a Shimadzu Solid Spec-3700 DUV spectrophotometer with $BaSO_4$ as a reference with the reflectance of 100%. The IR spectra was acquired on a Nicolet Magana 750 FT-IR spectrophotometer in the range of 2.5–25 μm.

SHG and Laser Induced Damage Threshold (LIDT). Powder SHG was measured using the Kurtz and Perry method with Q-switched Nd:YAG lasers at wavelengths of 1064 and 532 nm. Polycrystalline samples were ground and sieved into a series of distinct size ranges, namely, 25–45, 45–75, 75–109, 109–150, and 150–212 μm, and KDP and BBO sieved into the same size ranges were used as references. The powder LIDT measurements were taken using a Nd:YAG nanosecond laser at 1064 nm with a pulse duration of 10 ns, and the spot diameter was 1.20 mm. Polycrystalline samples were ground into particle sizes of 150–212 μm, and KDP sieved into the same size ranges were used as the reference.

Birefringence Measurements. The birefringence of crystalline sample $NRPF{\cdot}H_2O$ was assessed with a polarizing microscope ZEISS Axio Scope. A1 equipped with a Berek compensator. The wavelength of the light source was 546 nm. The birefringence was calculated according to Eqn. (1):

$$\Delta R \text{ (retardation)} = \Delta n \times T \qquad (1)$$

, where ΔR denotes the optical path difference, Δn represents the birefringence, and T is the thickness of the crystal. The positive and negative rotation of compensation affords the relative retardation. The

transparent (010)-NRPF·H_2O single crystal wafer were selected to scan under the polarizing microscope. The thickness of crystalline sample NRPF was measured on the Bruker PHOTON II CPAD detector (Fig. S5).

Theoretical calculations. Since Na and Rb atoms are disordered on the Wyckoff 2*a* site, three models with random occupation of metal atoms were established to find a reasonable structure. The model with the lowest calculated free energy is used for the corresponding calculations. A 1 × 1 × 1 cell containing 20 atoms (1 of 4 Na replaced by Rb) was built. Then the electronic structures and the linear and nonlinear optical properties of the title compounds were calculated by using the pseudopotential method in the VASP[S1] package and the density functional theory (DFT).[S2] The pseudopotentials were used to simulate the ion electron interaction of all constituent elements: Rb $4s^2 4p^6 5s^2$, Na $2p^6 3s^1$, P $3s^2 3p^3$, O $2s^2 2p^4$, F $2s^2 2p^4$, H $1s^1$. A kinetic energy cutoff of 500 eV was chosen with Monkhorst-Pack k-point meshes spanning less than 0.05/Å^3 in the Brillouin zone. And then we use the optimized structures to calculate the static self-consistency, the density of state and energy band with a dense 0.02/Å^3 *k*-point spacing mesh. According to the Kramers-Kronig transformation,[S3,4] the real part of the dielectric function $\varepsilon_1(\omega)$, the refractive index *n* and other linear optical properties can be calculated. Based on the so called length-gauge formalism derived by Aversa and Sipe,[S5,6] utilizing the specific calculation method invented by Professor Zhang, etc[S7] the SHG coefficients were calculated.

II. Tables and Figures

Table S1 Crystal data and structure refinement for NRPF·H_2O.

Compound	$Na_{1.5}Rb_{0.5}PO_3F·H_2O$
Formula weight	193.52
Crystal system	Orthorhombic
Crystal color	colorless
Space group	$Pmn2_1$ (no. 31)
a (Å)	6.0155(13)
b (Å)	8.9652(18)
c (Å)	4.9689(9)
$\alpha = \beta = \gamma$ (deg.)	90
V (Å^3)	267.97(9)
Z	2
D_c (g.cm^{-3})	2.398
μ (mm^{-1})	5.132
F(000)	186
GOOF on F^2	1.107
R_1, wR_2 ($I > 2\sigma(I)$)[a]	0.0218, 0.0562
R_1, wR_2 (all data)[a]	0.0233, 0.0575
Largest diff peak/hole (e·Å^{-3})	0.364, -0.424
Flack parameter	-0.041(13)

[a] $R_1 = \Sigma||F_o| - |F_c||/\Sigma|F_o|$ and $wR_2 = [\Sigma w(F_o^2 - F_c^2)^2/\Sigma w(F_o^2)^2]^{1/2}$ for $F_o^2 > 2\sigma(F_o^2)$

Table S2 Atomic coordinates and equivalent isotropic displacement parameters for NRPF·H_2O.

Atom	Ox.	Wyck.	Site Occ.	*x/a*	*y/b*	*z/c*	U_{eq} (Å^2)[a]
Rb1	+1	2*a*	0.503	0.5000(0)	0.4436(1)	0.8409(1)	0.024(1)
Na1	+1	2*a*	0.497	0.5000(0)	0.4436(1)	0.8409(1)	0.024(1)
Na	+1	2*a*	1.000	0.5000(0)	0.0368(2)	0.7319(3)	0.020(1)
P	+5	2*a*	1.000	0.5000(0)	0.7790(1)	0.3498(2)	0.013(1)
O1	-2	2*a*	1.000	0.5000(0)	0.6120(3)	0.3430(9)	0.028(1)
O2	-2	4*b*	1.000	0.7082(3)	0.8476(2)	0.4605(4)	0.023(1)
F	-1	2*a*	1.000	0.5000(0)	0.8260(3)	0.0388(5)	0.028(1)
O_w	-2	2*a*	1.000	0.5000(0)	0.2219(3)	0.3850(6)	0.025(1)
H	+1	4*b*	1.000	0.6130(5)	0.1965(0)	0.2960(9)	0.070(1)

[a] U_{eq} is defined as one-third of the trace of the orthogonalized U_{ij} tensor.

Table S3 Selected distances (Å) and angles (deg.) of NRPF·H_2O.

P–O(1)	1.498(2)	Rb(1)–O(1)	2.898(4)
P–O(2)	1.4998(18)	Rb(1)–O(1)#1	2.916(4)
P–O(2)#5	1.4998(18)	Rb(1)–O_w	3.014(3)
P–F	1.602(2)	Rb(1)–O(1)#2	3.0488(8)
Na–O(2)#3	2.333(2)	Rb(1)–O(1)#3	3.0488(8)
Na–O(2)#4	2.333(2)	Rb(1)–O(2)#4	3.201(2)
Na–O(2)#11	2.503(2)	Rb(1)–O(2)#3	3.201(2)
Na–O(2)#12	2.503(2)	Rb(1)–O_w#1	3.356(3)
Na–O_w	2.393(3)	Rb(1)–F#1	3.566(3)
Na–F	2.428(3)	O(1)#1–Rb(1)–O(1)#3	94.69(9)
O(1)–P–O(2)	114.70(11)	O_w–Rb(1)–O(1)#3	83.95(7)
O(1)–P–O(2)#5	114.70(11)	O(1)#2–Rb(1)–O(1)#3	161.17(9)
O(2)–P–O(2)#5	113.27(17)	O(1)–Rb(1)–O(2)#4	125.67(6)
O(1)–P–F	104.0(2)	O(1)#1–Rb(1)–O(2)#4	105.27(6)
O(2)–P–F	104.25(10)	O_w–Rb(1)–O(2)#4	66.52(6)
O(2)#1–P–F	104.25(10)	O(1)#2–Rb(1)–O(2)#4	47.56(6)
O(2)#3–Na–O(2)#4	97.56(11)	O(1)#3–Rb(1)–O(2)#4	114.01(6)
O(2)#3–Na–O_w	92.45(8)	O(1)–Rb(1)–O(2)#3	125.67(6)
O(2)#4–Na–O_w	92.45(8)	O(1)#1–Rb(1)–O(2)#3	105.27(6)
O(2)#3–Na–F#10	92.30(8)	O_w–Rb(1)–O(2)#3	66.52(6)
O(2)#4–Na–F#10	92.30(8)	O(1)#2–Rb(1)–O(2)#3	114.01(6)
O_w–Na–F#10	172.80(12)	O(1)#3–Rb(1)–O(2)#3	47.56(5)
O(2)#3–Na–O(2)#11	160.00(7)	O(2)#4–Rb(1)–O(2)#3	66.49(6)
O(2)#4–Na–O(2)#11	100.77(5)	O(1)–Rb(1)–O_w#1	175.05(9)
O_w–Na–O(2)#11	94.69(10)	O(1)#1–Rb(1)–O_w#1	67.51(8)
F#10–Na–O(2)#11	79.09(8)	O_w–Rb(1)–O_w#1	102.40(8)
O(2)#3–Na–O(2)#12	100.77(5)	O(1)#2–Rb(1)–O_w#1	84.28(7)
O(2)#4–Na–O(2)#12	160.00(8)	O(1)#3–Rb(1)–O_w#1	84.28(7)
O_w–Na–O(2)#12	94.69(10)	O(2)#4–Rb(1)–O_w#1	50.75(5)
F#10–Na–O(2)#12	79.09(8)	O(2)#3–Rb(1)–O_w#1	50.75(5)
O(2)#11–Na–O(2)#12	60.05(9)	O(1)–Rb(1)–F#1	74.62(7)
O(1)–Rb(1)–O(1)#1	117.44(8)	O(1)#1–Rb(1)–F#1	42.82(7)
O(1)–Rb(1)–O_w	72.65(8)	O_w–Rb(1)–F#1	147.27(7)
O(1)#1–Rb(1)–O_w	169.91(9)	O(1)#2–Rb(1)–F#1	98.99(5)
O(1)–Rb(1)–O(1)#2	95.05(9)	O(1)#3–Rb(1)–F#1	98.99(5)
O(1)#1–Rb(1)–O(1)#2	94.69(9)	O(2)#4–Rb(1)–F#1	137.11(4)
O_w–Rb(1)–O(1)#2	83.95(7)	O(2)#3–Rb(1)–F#1	137.11(4)
O(1)–Rb(1)–O(1)#3	95.05(9)	O_w#1–Rb(1)–F#1	110.33(7)

Symmetry codes: #1 x, y, z + 1; #2 *-x* + 1/2, *-y* + 1, *z* + 1/2; #3 *-x* + 3/2, *-y* + 1, *z* + 1/2; #4 *x* - 1/2, *-y* + 1, *z* + 1/2; #5 *-x* + 1, *y*, *z*; #6 *x*, *y* - 1, *z* + 1; #7 *-x* + 1, *y* - 1, *z*; #8 *x*, *y* - 1, *z*.

Table S4 Anisotropic displacement parameters (Å^2) for NRPF·H_2O. The anisotropic displacement factor exponent takes the form: $-2\pi^2[h^2a^{*2}U_{11} + ... + 2hka^*b^*U_{12}]$.

Atom	U_{11}	U_{22}	U_{33}	U_{23}	U_{13}	U_{12}
Rb1	0.023(1)	0.025(1)	0.023(1)	-0.001(1)	0	0
Na1	0.023(1)	0.025(1)	0.023(1)	-0.001(1)	0	0
Na	0.020(1)	0.019(1)	0.019(1)	-0.002(1)	0	0
P	0.012(1)	0.014(1)	0.012(1)	0	0	0
O1	0.038(1)	0.031(1)	0.031(1)	-0.002(2)	0	0
O2	0.016(1)	0.034(1)	0.021(1)	0	-0.002(1)	-0.008(1)
F	0.035(1)	0.038(1)	0.012(1)	0.007(1)	0	0
O_w	0.027(2)	0.030(1)	0.017(2)	0.001(1)	0	0

Table S5 Hydrogen bonds (Å) of N–H···O, O–H···O and N–H···F in compound NPF·H_2O.[S8]

D–H···A	D–H (Å)	H···A (Å)	D–H···A (°)
N1–H1···O1^{i}	0.8801	1.9923	167.7142
N1–H2···O_w4^{ii}	0.9586	1.8694	164.2923
N1–H3···O2^{iii}	0.8846	2.0394	171.9892
N1–H4···O3^{iii}	0.9563	1.8815	169.1982
N2–H5···O1^{i}	0.8756	2.0123	167.3962
N2–H6···O3^{i}	0.7344	2.1023	172.1413
N2–H7···O2^{iv}	0.8697	1.9449	173.2013
N2–H8···O1^{iii}	0.9144	1.9816	172.1532
O_w4–H9···O2^{iii}	0.8202	1.9320	169.8214
O_w4–H10···O3^{iii}	0.8306	1.9792	170.8733
N2–H5···F1^{a}	0.8756	2.6439	127.3342
N2–H7···F1^{a}	0.8697	2.8411	116.2002

Symmetry codes: (i) $-x + 1, y - 1/2, -z + 1/2$; (ii) $x, -y + 1/2, z - 1/2$; (iii) x, y, z; (iv) $x, -y + 1/2, z + 1/2$. ^{a}: weak hydrogen bond.

Table S6 Hydrogen bonds (Å) of O–H···O, O–H···F and N–H···F in compound NNPF·H_2O.[S9]

D–H···A	D–H (Å)	H···A (Å)	D–H···A (°)
N1–H1···O3^{i}	0.8756	2.0123	167.3962
N1–H2···O3^{ii}	0.7344	2.1023	172.1413
N1–H3···O3^{iii}	0.8697	1.9449	173.2013
N1–H4···O2^{iv}	0.9144	1.9816	172.1532
O_w4–H5···O1^{i}	0.8202	1.9320	169.8214
O_w4–H6···O2^{iv}	0.8306	1.9792	170.8733
O_w4–H5···F1^{a}	0.8202	2.6291	115.4995
O_w4–H6···F1^{a}	0.8306	2.7484	116.7044
N1–H3···F1^{a}	0.8697	2.8309	126.6172

Symmetry codes: (i) x + 1/2, -y + 1, z + 1/2; (ii) x, y, z; (iii) x, y, z + 1; (iv) x - 1/2, -y + 1, z + 1/2. ^{a}: weak hydrogen bond.

Table S7 Hydrogen bonds (Å) of O–H···O and O–H···F in compound NRPF·H_2O.

D–H···A	D–H (Å)	H···A (Å)	D–H···A (°)
O_w–H···O2^{i}	0.8435	2.0221	156.074
O_w–H···F^{a}	0.8435	2.6294	119.5752

Symmetry codes: (i) -x + 3/2, -y + 1, z - 1/2. ^{a}: weak hydrogen bond.

Table S8 Contribution of each chemical bond to the largest SHG coefficient d_{36} in (a) ADP and (b) KDP.[S10]

(a)

Compound	SHG coefficient	H^N–N	H^N–O(s)	H^N–O(l)	H–O(s)	H–O(l)	P–O
ADP	d_{36} / (10^{-9} esu)	-0.752	1.084	1.394	0	0	0.008

(b)

Compound	SHG coefficient	K–O(l)	K–O(s)	H–O(s)	H–O(l)	P–O
KDP	d_{36} / (10^{-9} esu)	-0.022	0.016	0	0	0.955

H^N presents H connected to N. O(s) and O(l) present short and long distance of O, respectively.

Table S9 Direction and magnitude of dipole moments of $[PO_3F]^{2-}$ groups in NRPF·H_2O, NNPF·H_2O,[S9] NPF·H_2O[S8] and Na_2PO_3F[S11] in one unit cell.

Compound	Anion	μ_x (Debye)[a]	μ_y (Debye)[a]	μ_z (Debye)[a]	Total (Debye)[b]
NRPF·H_2O	$PO_3F(1)$	0.0079	-0.3945	-1.0763	1.1464
	$PO_3F(2)$	0	0.3945	-1.0763	1.1464
	Sum	0.0079	0	-2.1526	**2.1526**[c]
NNPF·H_2O	$PO_3F(1)$	-1.3153	0.4360	0.0528	1.3867
	$PO_3F(2)$	-1.3153	-0.4360	0.0528	1.3867
	Sum	2.6306	0	0.1056	**2.6327**[c]
NPF·H_2O	$PO_3F(1)$	0.2976	1.0051	0.9558	1.4185
	$PO_3F(2)$	0.2976	-1.0051	0.9558	1.4185
	$PO_3F(3)$	-0.2976	1.0051	-0.9558	1.4185
	$PO_3F(4)$	-0.2976	-1.0051	-0.9558	1.4185
	Sum	0	0	0	**0**[c]
Na_2PO_3F	$P1O_3F(1)$	0.5526	1.1405	-0.3226	1.3077
	$P1O_3F(2)$	-0.5526	-1.1405	-0.3226	1.3077
	$P1O_3F(3)$	-0.5526	1.1405	0.3226	1.3077
	$P1O_3F(4)$	0.5526	-1.1405	0.3226	1.3077
	$P2O_3F(1)$	-0.1442	1.7464	-0.2291	1.7673
	$P2O_3F(2)$	0.1442	-1.7464	-0.2291	1.7673
	$P2O_3F(3)$	-0.1442	-1.7464	0.2291	1.7673
	$P2O_3F(4)$	0.1442	1.7464	0.2291	1.7673
	Sum	0	0	0	**0**[c]

[a]Calculated according to the equation $\mu = neR$; μ is the dipole moment, n = total number of electrons, e = charge on the electron -4.8×10^{-10} esu, R = difference (in cm) between the center of mass of the protons and electrons; 1debye unit = 10^{-18} esu cm.

[b]Total = $(x^2 + y^2 + z^2 + 2xy\cos\gamma + 2xz\cos\beta + 2yz\cos\alpha)^{1/2}$; α, β and γ are crystal unit cell parameters.

[c]Sum = $\left(\left(\sum_{i=1}^{n}\mu_x\right)^2 + \left(\sum_{i=1}^{n}\mu_y\right)^2 + \left(\sum_{i=1}^{n}\mu_z\right)^2\right)^{1/2}$

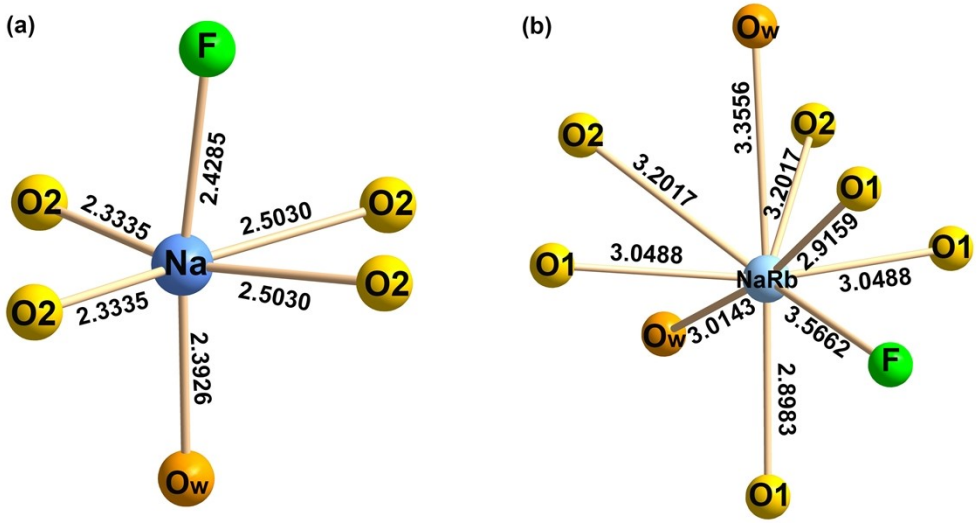

Fig. S1 Distorted coordination environment of (a) Na^+ and (b) Na^+/Rb^+ in NRPF·H_2O.

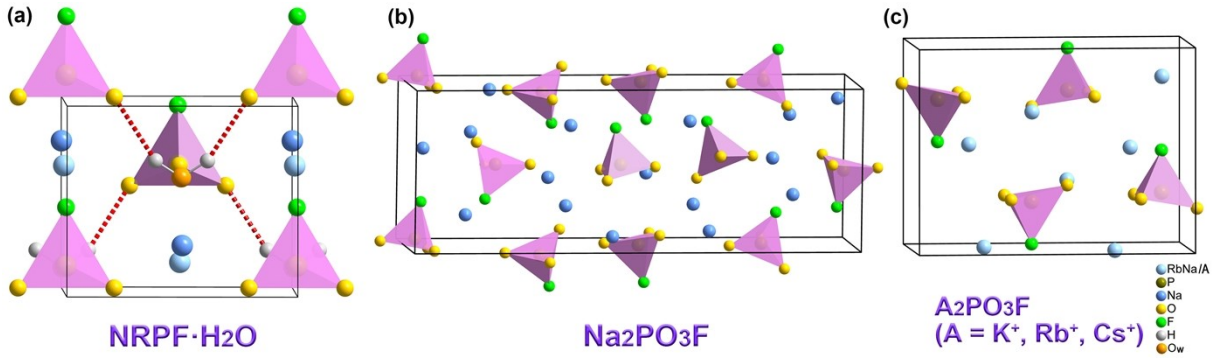

Fig. S2 H_2O molecules act as the structural regulator on the spatial arrangement of $[PO_3F]^{2-}$ groups in one unit. (a) NRPF·H_2O. (b) Na_2PO_3F. (c) A_2PO_3F (A = K^+, Rb^+, Cs^+).

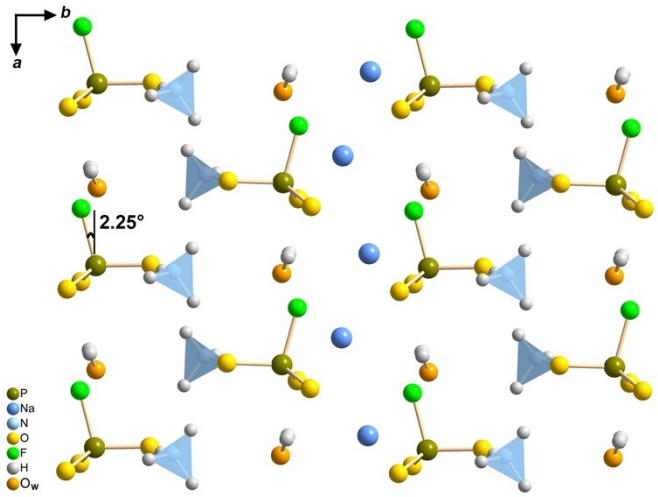

Fig. S3 P–F bond is off the *a* axis by an angle of 2.25° in NNPF·H_2O.

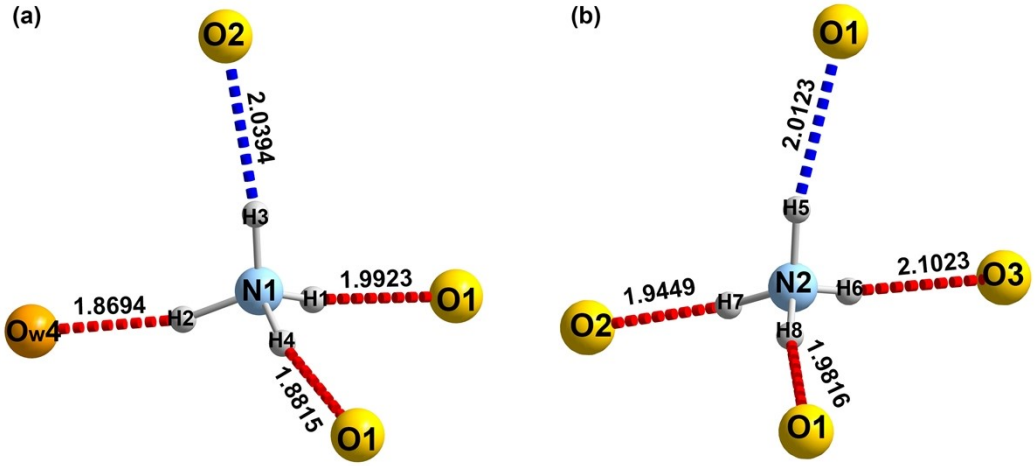

Fig. S4 Hydrogen-bond coordination environment around (a) $N1H_4^+$ and (b) $N2H_4^+$ in NPF·H_2O.

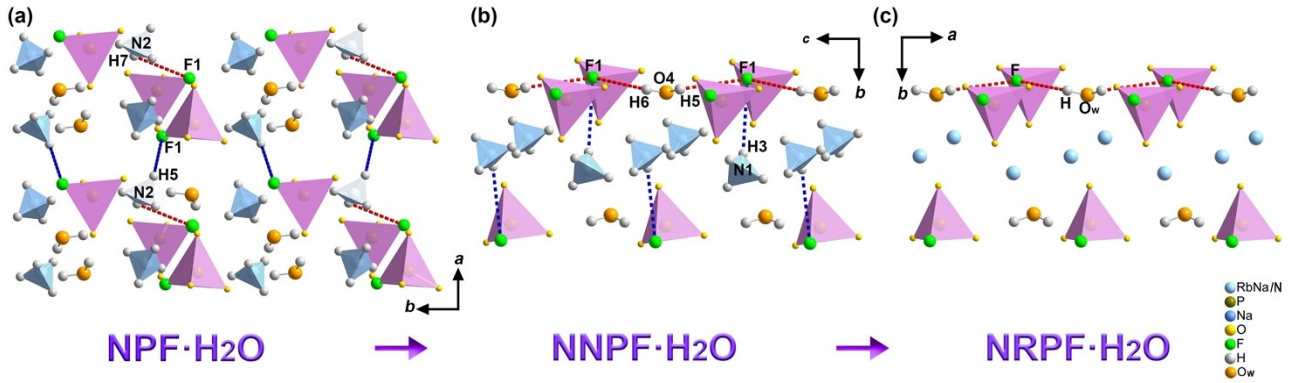

Fig. S5 Comparison of weak hydrogen bonds of O–H···F and N–H···F within NPF·H_2O, NNPF·H_2O and NRPF·H_2O.

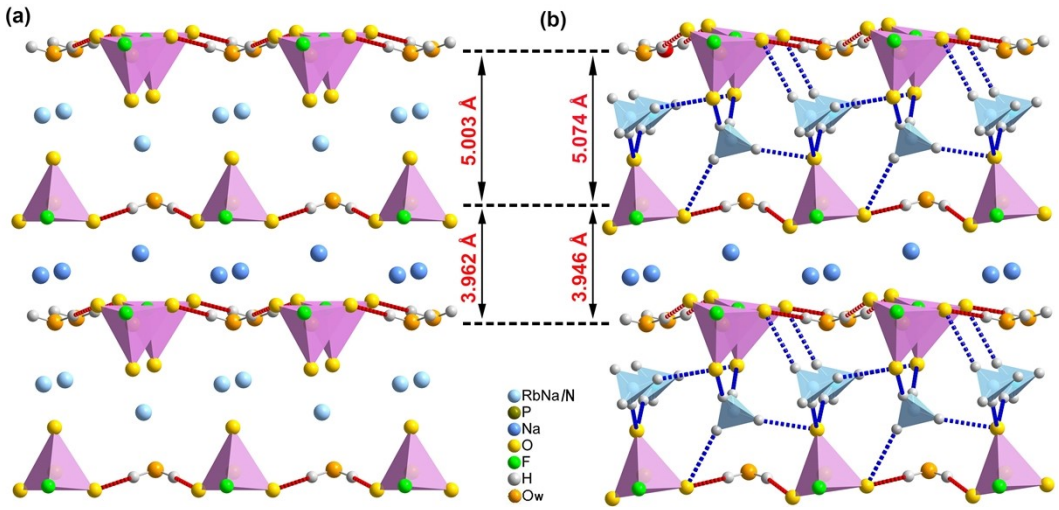

Fig. S6 Inter-layer distances of (a) NRPF·H_2O and (b) NNPF·H_2O.

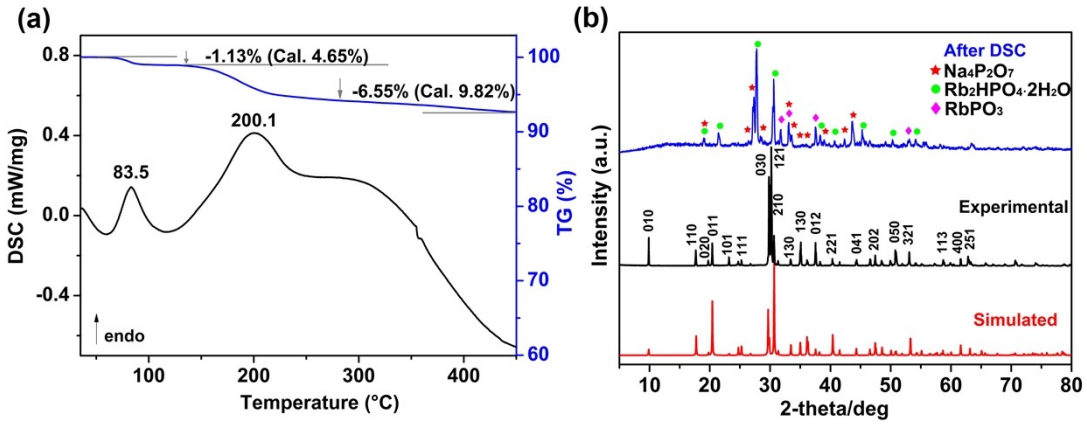

Fig. S7 DSC, TG curves and the PXRD patterns for NRPF·H_2O before and after the DSC measurement.

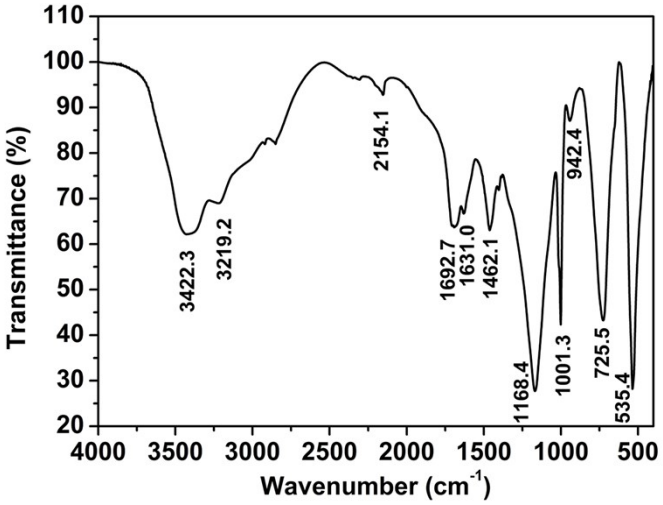

Fig. S8 IR spectrum for NRPF·H_2O.

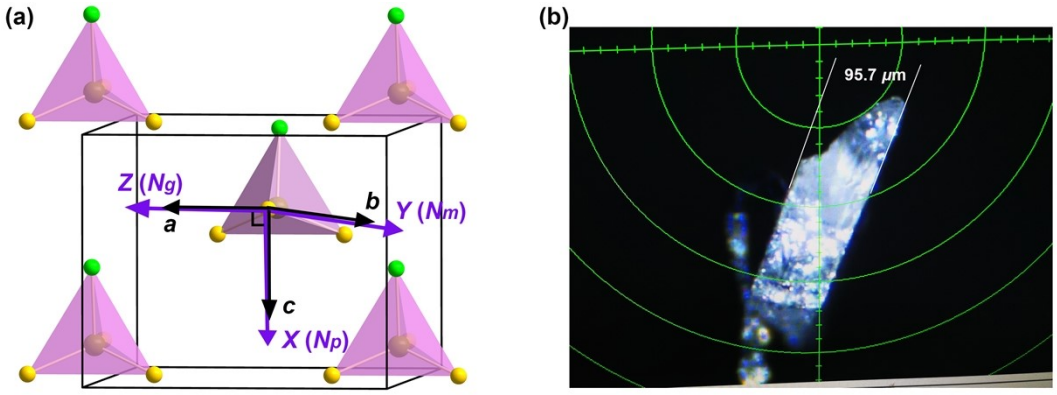

Fig. S9 (a) Correlation between the crystallographic and crystallophysical axes in NRPF·H_2O, *a* // *Z*, *b* // *Y* and *c* // *X*. (b) Thickness of the (010)-NRPF·H_2O single crystal wafer measured on the Bruker PHOTON II CPAD detector for the birefringence measurement.

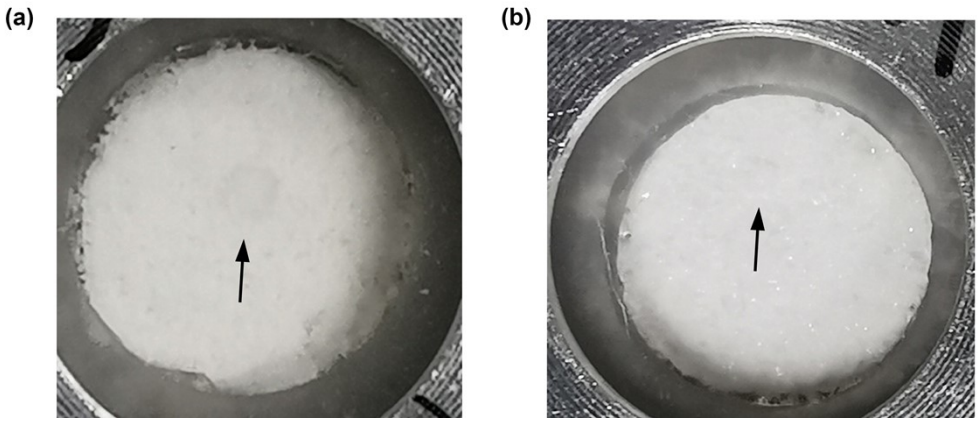

Fig. S10 LIDT measurement on the polycrystalline (a) NRPF·H_2O and (b) KDP with the same size ranges of 150–212 μm.

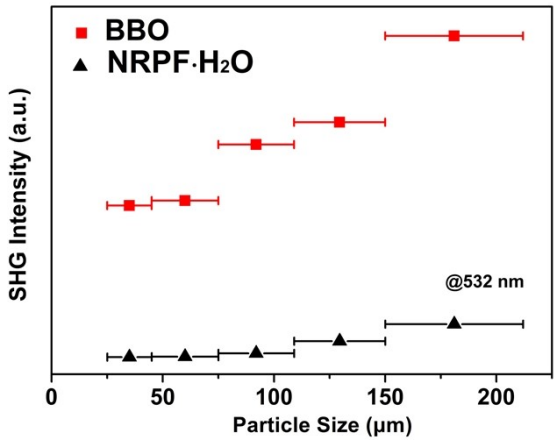

Fig. S11 Phase-matching curves and SHG intensity at the incident wavelength of 532 nm with BBO as a reference of polycrystalline NRPF·H_2O.

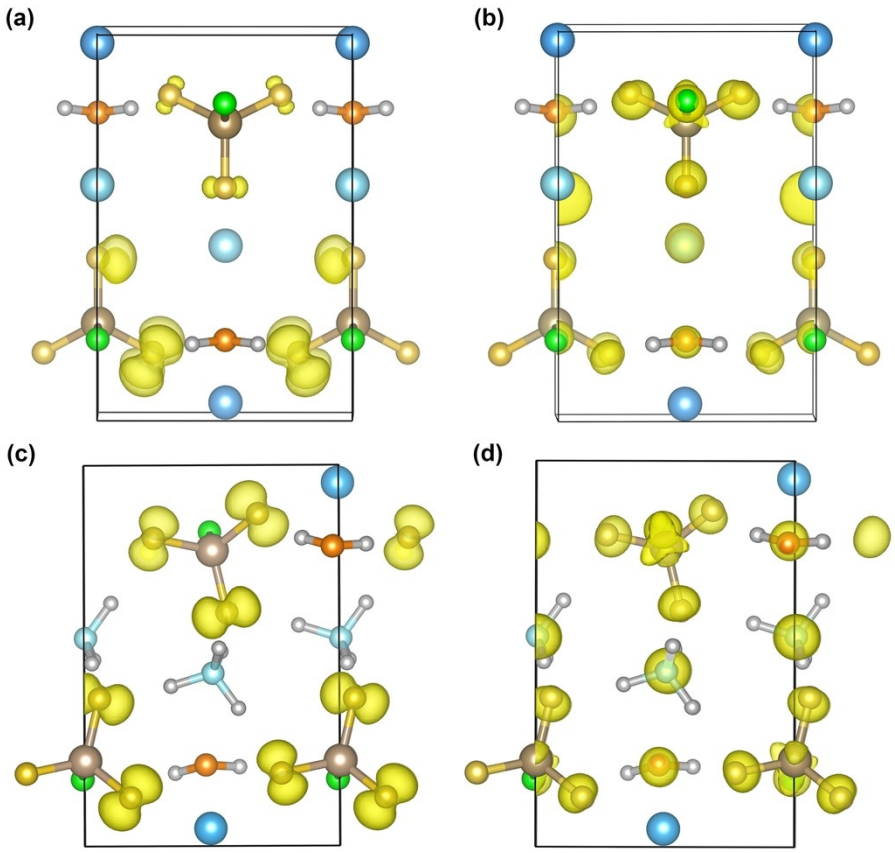

Fig. S12 Electron density distribution in the (a) VBM and (b) CBM of NRPF·H_2O, (c) VBM and (d) CBM of NNPF·H_2O.

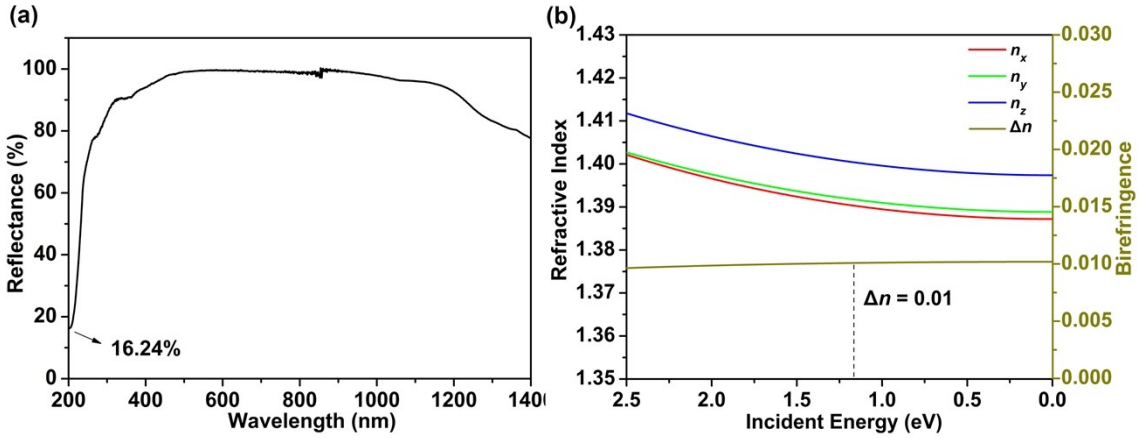

Fig. S13 (a) UV–vis–NIR diffuse reflectance spectrum and (b) calculated dispersion of the refractive indices and birefringence of $NPF \cdot H_2O$.

References

(S1) G. Kresse and J. Furthmuller, Efficient iterative schemes for ab initio total-energy calculations using a plane-wave basis set, *Phys. Rev. B.*, 1996, **54**, 11169–11186.

(S2) W. Kohn, Electronic structure of matter-wave functions and density functions, *Rev. Mod. Phys.*, 1999, **71**, 1253–1266.

(S3) S. Laksari, A. Chahed, N. Abbouni, O. Benhelal and B. Abbar, First-principles calculations of the structural, electronic and optical properties of $CuGaS_2$ and $AgGaS_2$, *Comp. Mater. Sci.*, 2006, **38**, 223–230.

(S4) S. D. Mo and W. Y. Ching, Electronic and optical properties of three phases of titanium dioxide: rutile, anatase, and brookite, *Phys. Rev. B.*, 1995, **51**, 13023–13032.

(S5) C. Aversa and J. E. Sipe, Nonlinear optical susceptibilities of semiconductors: results with a length-gauge analysis, *Phys. Rev. B.*, 1995, **52**, 14636–14645.

(S6) S. N. Rashkeev, W. R. L. Lambrecht and B. Segall, Efficient ab initio method for the calculation of frequency-dependent second-order optical response in semiconductors, *Phys. Rev. B.*, 1998, **57**, 3905–3919.

(S7) Z. X. Fang, J. Lin, R. Liu, P. Liu, Y. Li, X. Huang, K. Ding, L. X. Ning and Y. F. Zhang, Computational design of inorganic nonlinear optical crystals based on a genetic algorithm, *Cryst. Eng. Comm.*, 2014, **16**, 10569–10580.

(S8) A. Perloff, The crystal structures of hydrated calcium and ammonium monofluorophosphates: $CaPO_3F{\cdot}2H_2O$ and $(NH_4)_2PO_3F{\cdot}H_2O$, *Acta Crystallogr., Sect. B: Struct. Crystallogr. Cryst. Chem.*, 1972, **B28**, 2183–2191.

(S9) J. Lu, J. N. Yue, L. Xiong, W. K. Zhang, L. Chen and L. M. Wu, Uniform alignment of non-π-conjugated species enhances deep ultraviolet optical nonlinearity, *J. Am. Chem. Soc.*, 2019, **141**, 8093–8097.

(S10) S. Y. Zhang, Dielectric theory of complex crystalline chemical-bond and its application, *Science Press.*, 2005, 65–66.

(S11) J. Durand, L. Cot and J. L. Galigné, Etudes structurales de composés oxyfluorés du P^V. II. structure cristalline de Na_2PO_3F β, *Acta Crystallogr., Sect. B: Struct. Crystallogr. Cryst. Chem.*, 1974, **B30**, 1565–1569.